POLITECNICO DI TORINO
Repository ISTITUZIONALE

Terahertz Multiple Access: A Deep Reinforcement Learning Controlled Multihop IRS Topology

(Article begins on next page)

06 July 2024

Terahertz Multiple Access: A Deep Reinforcement Learning Controlled Multihop IRS Topology

MUHAMMAD SHEHAB[1] **(Member, IEEE), MOHAMED ELSAYED**[2] **(Member, IEEE),**
ABDULLATEEF ALMOHAMAD[2] **(Member, IEEE), AHMED BADAWY**[3] **(Member, IEEE),**
TAMER KHATTAB[2] **(Senior Member, IEEE), NIZAR ZORBA**[2] **(Senior Member, IEEE),**
MAZEN HASNA[2] **(Senior Member, IEEE), AND DANIELE TRINCHERO**[1]

[1]Dipartimento di Elettronica, Politecnico di Torino, 10129 Turin, Italy

[2]Electrical Engineering, Qatar University, Doha, Qatar

[3]Computer Science and Engineering, Qatar University, Doha, Qatar

CORRESPONDING AUTHOR: A. BADAWY (e-mail: badawy@qu.edu.qa)

ABSTRACT We explore THz communication uplink multi-access with multi-hop Intelligent reflecting surfaces (IRSs) under correlated channels. Our aims are twofold: 1) enhancing the data rate of a desired user while dealing with interference from another user and 2) maximizing the combined data rate. Both tasks involve non-convex optimization challenges. For the first aim, we devise a sub-optimal analytical approach that focuses on maximizing the desired user's received power, leading to an over-determined system. We also attempt to use approximate solutions utilizing pseudo-inverse (P_{inv}) and block solution (*BLS*) based methods. For the second aim, we establish a loose upper bound and employ an exhaustive search (*ES*). We employ deep reinforcement learning (DRL) to address both aims, demonstrating its effectiveness in complex scenarios. DRL outperforms mathematical approaches for the first aim, with the performance improvement of DDPG over the block solution ranging from 8% to 57.12%, and over the pseudo-inverse ranging from 41% to 190% for a correlation-factor equal to 1. Moreover, DRL closely approximates the *ES* for the second aim. Furthermore, our findings show that as channel correlation increases, DRL's performance improves, capitalizing on the correlation for enhanced statistical learning.

INDEX TERMS Artificial intelligence, multi-access communication, sub-millimeter wave communication, communication system performance.

I. INTRODUCTION

IN THE field of wireless communication, 6G is expected to cater to significantly advanced services and data-intensive applications compared to its predecessor, 5G. These applications, such as immersive remote presence, connected robotics (CRAS), digital twins, and immersive extended reality (XR), necessitate a colossal 1000-fold increase in capacity compared to 5G mobile systems [1]. To address these demands and reconcile the tension between service needs and limited spectrum resources [2], there is a call to extend existing wireless spectrum bands and venture into the higher terahertz (THz) frequency range, spanning from 0.1 THz to 10 THz. These frequencies are poised to play a pivotal role in 6G wireless communications due to their potential for substantially enhanced capacities and data rates. However, these higher Radio Frequencies (RF) bring challenges such as substantial path attenuation, elevated propagation losses, and intermittent wireless connections. Moreover, RF waves with extremely short wavelengths result in limited communication distances and increased vulnerability to molecular absorption and obstruction [1]. To enhance received signal power and achievable data rates, this paper explores the Intelligent reflecting surfaces (IRS) as a burgeoning and highly promising technological advancement [3]. IRS operates by manipulating incident electromagnetic waves, programmatically adjusting phase

shifts of semi-passive reflecting elements to enable a smart radio environment, enhancing data rates in a cost-effective and energy-efficient manner [4].

II. LITERATURE REVIEW

Numerous recent studies have scrutinized the deployment of IRS in THz communications to evaluate its potential in improving coverage and achievable data rates [5], [6], [7], [8], [9], [10], [11]. For example, one study [5] focused on an IRS-assisted multi-hop multi-pair unicast network, where multiple sources communicate with multiple destinations, proposing distributed control of multiple IRSs to optimize achievable rates. Another study [6] explored a multi-IRS-assisted massive multiple-input multiple-output system, aiming to boost minimum received signal power. It involved a base station (BS) equipped with multi-antennas transmitting independent signals to remote users with single antennas, enabling cascaded line-of-sight (LOS) communication links through cooperative signal reflections from various IRS groups. In [7], the authors assessed the effectiveness of a decode-and-forward (DF) relaying assisted multi-IRS system in a scenario where a single source communicates with a single destination, seeking to determine the optimal IRS configuration, the number of IRSs, and the number of IRS reflecting elements that maximize the ergodic rate. Additionally, in [8], the authors considered a multi-hop IRS-assisted multi-user downlink communication scenario where the BS communicates with K users, optimizing the beamforming at the BS and multiple IRS phase shift reflection matrices to maximize the sum rate. Furthermore, in [9], the authors explored an uplink multi-hop IRS communication system where multiple users communicate with a single destination, to extend the link range in THz communications and maximize power at the receiver (R_x). They introduced a cascaded passive IRS THz system to overcome the substantial propagation losses due to air molecule absorption.

Notably, the studies from [5] to [9] employed mathematical techniques to address their optimization problems. In contrast, research papers [10] and [11] utilized the DRL algorithm to tackle non-convex optimization challenges. The authors suggested a hybrid beamforming scheme for multi-hop IRS-aided networks to enhance the coverage of THz communication links. They investigated the joint design of analog beamforming at the IRSs and digital beamforming at the BS to mitigate propagation losses in THz downlink broadcast systems, which involve a single source and multiple destinations.

A. CONTRIBUTIONS

To enhance the range of THz links and compensate for losses at such high frequencies, we employ multi-hop IRS, often referred to as cascaded IRSs, as a fundamental element in our system model. Given the limited coverage typically associated with THz links, we focus on small areas where multiple users are not expected. Our optimization problem centers around a two-user system, to find the optimal phase shifts for the multi-hop IRS elements. This optimization aims to maximize the received rate for a specific user and the combined rate for both users. The primary challenge in our approach arises from the non-convex nature of the objective function due to constraints related to the constant amplitude of the IRS reflecting elements, as well as non-linear constraints and complex multi-hop links. Solving this NP-hard problem optimally remains elusive, and conventional mathematical techniques struggle to provide an analytical solution. Moreover, an exhaustive search (ES) approach is impractical for large-scale communication systems [10], [11]. Additionally, optimizing R_x rates leads to an over-determined system. To address these combined challenges, we employ DRL, specifically utilizing a Deep Deterministic Policy Gradient (DDPG) based scheme. This approach allows us to obtain efficient and feasible solutions. To the best of our knowledge, no prior studies in the existing literature have utilized the DRL approach to tackle the challenge of solving over-determined systems of equations in uplink cascaded IRS multiple access scenario. In this research, our objective is to address the existing gap in the literature by utilizing DDPG to simultaneously tune the phases of every individual IRS within the cascaded IRS system. We specifically consider the scenario of spatially correlated channels [12] between IRS$_1$ and IRS$_2$. We aim to approach two alternative scenarios, each with a different objective: a) maximizing the rate for any specific user, or b) maximizing the sum rate for both users.

We detail our contributions below against our two main objectives (two alternative scenarios), where both scenarios consider multi-hop IRSs and multiple access systems operating in the THz range:

- *Scenario 1:* Maximize the data rate for a single user, considering the second user as an interferer.
  - We formulate the optimization problem for the cascaded IRS phase shifts, encompassing IRS$_1$ and IRS$_2$, and establish that it is non-convex and computationally challenging.
  - Noticing the over-determined nature of this problem, we present two sub-optimal solutions to determine the ideal phase shift matrices of IRS$_1$ and IRS$_2$ that optimize the received power for the desired user, utilizing pseudo-inverse P_{inv} and block solutions (*BLS*).
  - We develop a DDPG scheme to obtain the ideal phase shifts for the desired user and compare its performance against the sub-optimal state-of-art schemes, as shown in Table 1.
- *Scenario 2:* Maximize the combined data rate for two users.
  - We provide analytical insights into this problem, specifically for cascaded IRSs.
  - We design a DDPG algorithm to calculate the ideal phase shifts for the cascaded IRSs that optimize the total data rate

TABLE 1. Comparing pseudo-inverse with block solution and DDPG.

| Feature	Pseudo-Inverse	Block Solution	DDPG
Complexity	High	Medium	Low
Adaptability	Static Configuration	Static Configuration	Dynamic Learning
Objective 1 (Rate of Desired User)	Sub-optimal	Decent Performance	Superior
Objective 2 (Sum Rate)	N/A	N/A	Near-optimal (Close to ES)
Handling Non-Convexity	Not suitable	Not suitable	Effective
Learning from Environment	No	No	Yes
Channel Correlation Impact	Low	Moderate	Significant
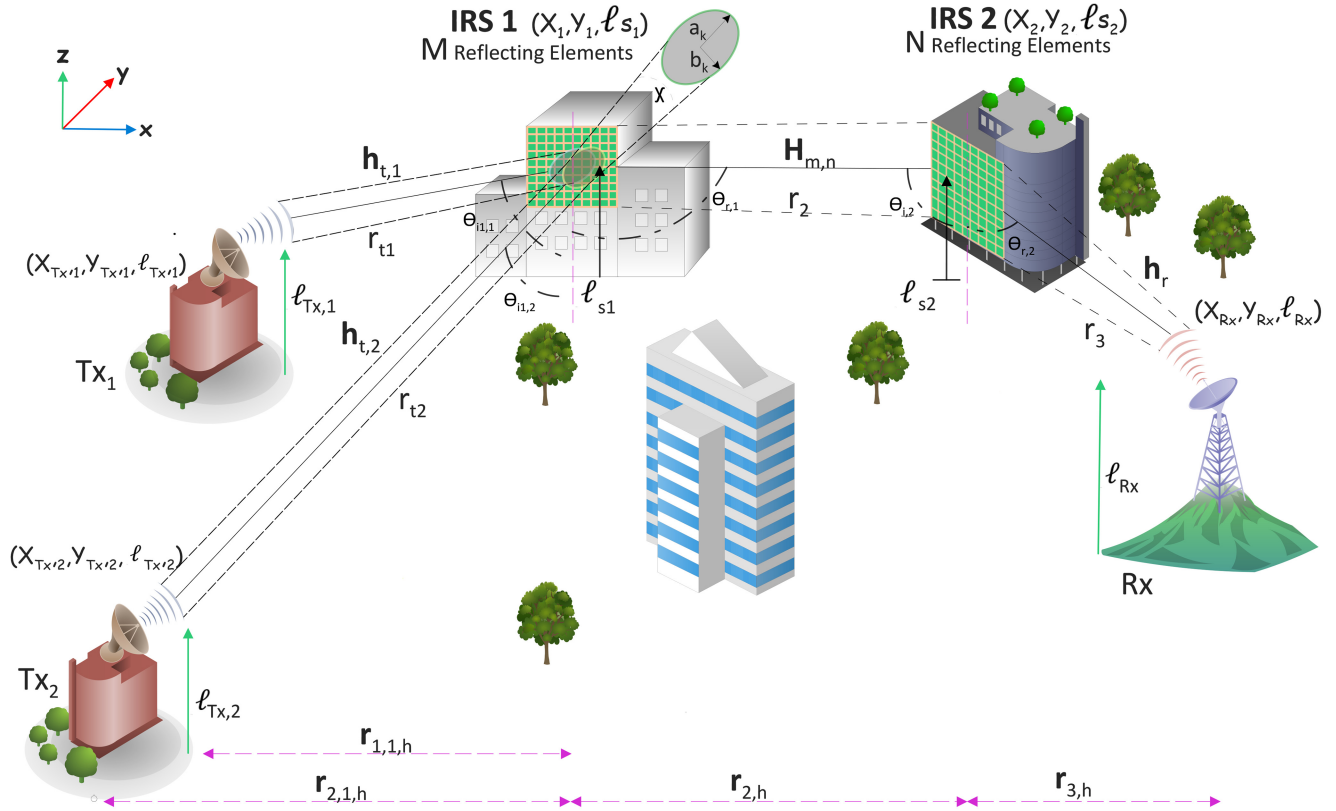
FIGURE 1. Cascaded IRS system model.

• We then simulate and compare the results obtained for both scenarios. We benchmark these results against an upper bound derived from *ES* and a lower bound generated from randomly assigned phase shifts.

The subsequent sections of this research paper are organized as follows: In Section II, we delve into the system and channel model concerning the multi-hop IRS scenario. Section III delves into the problem formulation, focusing on maximizing the data rate for the desired user while dealing with interference, while in Section IV, we explore the problem of maximizing the total data rate for both users. Here, we derive the end-to-end sum rate within the cascaded IRS scenario. Moving on to Section V, we introduce our proposed solution that employs the DDPG algorithm for controlling the phase shifts of the cascaded IRS. Numerical simulations, which shed light on our findings, are the subject of discussion in Section VI. Lastly, in Section VII, we draw our conclusion.

Notation: For more convenience, frequent symbols and parameters along with their description are illustrated in Table 2.

III. SYSTEM MODEL

In our system model, we consider an uplink multi-hop IRS communication system operating in the THz frequency range, depicted in Figure 1. Within this system, we have two users, each equipped with a single antenna. Notably, the communication process is facilitated by highly directional parabolic antennas employed by both users to transmit signals precisely focused at the center of IRS$_1$. Subsequently, these signals undergo reflection by the IRS$_1$ elements, followed by a secondary reflection from IRS$_2$ before reaching the final destination at R_x. The choice of THz frequencies is deliberate, primarily due to their suitability for scenarios with limited coverage areas—perfect for users 1 and 2. To mitigate the significant THz propagation losses caused by absorption in the air molecules we implemented a cascaded

TABLE 2. List of frequently used parameters and symbols.

Parameters and Symbols	Description
x_k	Transmitted signal for each user k
y_k	Received signal for each user k
z_k	Signal for each user k
P_t	Transmit power for each user
λ	Wavelength
$\mathbf{h}_r$	Channel between IRS_2 and the receiver
$\mathbf{H}_{m,n}$	Channel between IRS_1 and IRS_2
$\mathbf{h}_{t,k}$	Channel between each user k and IRS_1
n_0	AWGN in linear scale
K_1, K_2	Rician Factor for the transmitter channel and receiver channel
$\mathbf{R}$	Covariance Matrix
$\mathbf{\Phi}_M, \mathbf{\Phi}_N$	Phase shift reflection matrix for IRS_1 and IRS_2, respectively
ϕ_m, ϕ_n	Phase shift of IRS_1 reflecting element m and IRS_2 reflecting element n, respectively
η_m	Phase shift of mth IRS_1 reflecting element
ψ_n	Phase shift of nth IRS_2 reflecting element
D_t, D_r	Antenna diameters for each T_{x_k} and R_x, respectively
r_{tk}, r_2, r_3	Distance between: each user k and IRS_1, IRS_1 and IRS_2, and IRS_2 and R_x, respectively
$r_{k,1,h}, r_{2,h}, r_{3,h}$	Horizontal distance between: user k and center of IRS_1, centers of IRS_1 and IRS_2, and center of IRS_2 and R_x, respectively
$\theta_{ik,1}$	Incident angle from user k w.r.t. the center of the illuminated area at IRS_1
$\theta_{r,1}$	Reflected angle w.r.t. the center of the illuminated area at IRS_1
$\theta_{i,2}$	Incident angle from IRS_1 w.r.t. the center of the illuminated area at IRS_2
$\theta_{r,2}$	Reflected angle w.r.t. the center of the illuminated area at IRS_2
$\ell_{Tx,k}, \ell_{Rx}, \ell_{s1}, \ell_{s2}$	The height of the T_{x_k}, R_x, IRS_1 and IRS_2, respectively
M, N	Number of reflecting elements for IRS_1 and IRS_2 respectively
$[\mathbf{R}]_{m,n}$	Covariance matrix obtained based on the exponential spatial correlation model
$\rho^{|m-n|}$	Correlation-coefficient among the adjacent RUs
Ω_k	Phase shifts corresponding to signal traveled from user k to IRS_1
Ω_3	Phase shift corresponding to signal traveled from IRS2 to R_x
o	Angle measured from the broadside of the antenna
$G_t(o), G_r(o)$	Gains for the users' and receiver antennas respectively
$L_{\tau,k}$	Total losses and gains on the path between each T_{x_k} and the R_x
$L_{FSPL,\tau,k}$	Total FSPL for T_{x_k}
$L_{abs,\tau,k}$	Total absorption loss for T_{x_k}
$G_{t,k}\ G_r$	T_{x_k} , and R_x antenna gains
$G(\theta_{i1,k}), (\theta_{r,1})$	Gain of IRS_1 RU from the incident and reflection angles
$P_{r,m}$	The power reflected from the m_{th} RU of IRS_1
$P_{r,mn}$	The power reflected from the n_{th} RU of IRS2 because of being illuminated by the signal reflected by the m_{th} RU of IRS_1
$P_{rx,mn}$	The received captured power at the R_x
P_{Rx}	The total received power for user k at the receiver (R_x)
$\varphi_{t_{k_m}}$	The phase for the transmitter channel for user k and m^{th} RU
φ_{mn}	The phase for the $\mathbf{h}_{m,n}$ channel for m^{th} and n^{th} RU
φ_{r_n}	The phase for the receiver channel for $n^{th} RU$
γ_k	The received SINR for the T_{x_k} at the R_x
$R_k,$	The data rate for user k
R_{sum}	The sum rate for both users
$\Delta\Phi$	Phase Search Step

IRS system. Consequently, this setup effectively amplifies signal strength, particularly for signals facing challenges in traversing long distances due to their short wavelength and high frequency. The cascaded IRS configuration emerges as a strategic solution to enhance the overall robustness and efficiency of the communication process within the challenging THz spectrum. Further, each transmitter (T_x) and R_x is equipped with antennas having diameters of D_t and D_r respectively. The distances between various points in the system are defined as follows: r_{tk}, for the distance between the users and IRS_1, r_2 for the distance between IRS_1 and IRS_2, and r_3 for the distance between IRS_2 and the R_x. The horizontal distances between the transmitters and the center of IRS_1, IRS_1 and IRS_2, the center of IRS_2 and the R_x are denoted as $r_{k,1,h}$, $r_{2,h}$, and $r_{3,h}$, respectively. The angles of

incidence and reflection with respect to the center of the illuminated areas at IRS_1 and IRS_2 are represented by $\theta_{i1,1}$, $\theta_{i2,1}$, $\theta_{r,1}$, $\theta_{i,2}$, and $\theta_{r,2}$. The heights of the two transmitters, IRS_1, IRS_2, and the R_x are indicated as $\ell_{Tx,1}$, $\ell_{Tx,2}$, ℓ_{s1}, ℓ_{s2}, and ℓ_{Rx} respectively. The IRSs act as beamformers that focus the incoming signal at a particular reflection direction by modifying the phases of the reflecting units (RUs). The number of RUs in IRS_1 and IRS_2 are M and N respectively.

The transmitted signal for each user k, where $k \in 1, 2$, is represented by

$$x_k = \sqrt{P_t}z_k, \tag{1}$$

Here, z_k denotes the signal corresponding to user k and has a unit power (i.e., $\mathbb{E}[|z_k|^2] = 1$, $\mathbb{E}[.]$ designates the

expectation), and P_t represents the transmit power for each user. Thus, the received signal for each user k is

$$y_k = \mathbf{h}_r^H \boldsymbol{\Phi}_N \mathbf{H}_{m,n}^H \boldsymbol{\Phi}_M \mathbf{h}_{t,k}^H x_k + n_0,$$
$$y_k = \mathbf{h}_r^H \boldsymbol{\Phi}_N \mathbf{H}_{m,n}^H \boldsymbol{\Phi}_M \mathbf{h}_{t,k}^H \sqrt{P_t} z_k + n_0, \quad (2)$$

where $\mathbf{h}_{t,k} \in \mathbb{C}^{1 \times M}$ is the communication link between each user k and IRS$_1$; $\mathbf{H}_{m,n} \in \mathbb{C}^{M \times N}$ is the communication link between IRS$_1$ and IRS$_2$; $\mathbf{h}_r \in \mathbb{C}^{N \times 1}$ is the communication link between IRS$_2$ and the R_x; $\boldsymbol{\Phi}_M = \mathrm{diag}(e^{-j\eta_1}, e^{-j\eta_2}, \ldots, e^{-j\eta_M})$ and $\boldsymbol{\Phi}_N = \mathrm{diag}(e^{-j\psi_1}, e^{-j\psi_2}, \ldots, e^{-j\psi_N})$ are the phase shift reflection matrices for IRS$_1$ and IRS$_2$, respectively, that satisfy the constant modulus constraint on each diagonal element of the matrix, $|\phi_m|^2 = |e^{-j\eta_m}|^2 = 1, \forall m \in \{1, 2, \ldots, M\}, |\phi_n|^2 = |e^{-j\psi_n}|^2 = 1, \forall n \in \{1, 2, \ldots, N\}$; and diag(.) symbolizes the diagonal matrix. Moreover, the phase shifts of the mth and n^{th} reflecting elements are represented by η_m and ψ_n, where the values of η_m and ψ_n range between 0 and 2π, and the noise $n_0 \sim \mathcal{CN}(0, \sigma^2)$ denotes the AWGN for each user in linear scale. The deterministic phase shifts are associated with the distances that the signals from each user k travel during the first hop, as well as the link between IRS$_2$ and R_X during the third hop.

$$\Omega_k = 2\pi r_{t_k}/\lambda, \quad \text{and} \quad \Omega_3 = 2\pi r_3/\lambda, \quad (3)$$

where λ is the wavelength.

A. COMMUNICATION CHANNEL MODEL
The T_x and R_x channels $\mathbf{h}_{t,k}$, and $\mathbf{h}_r$ follow the Rician fading model [11], [13]

$$\mathbf{h}_{t,k} = \sqrt{\frac{K_1}{K_1 + 1}} \bar{\mathbf{h}}_{t,k} + \sqrt{\frac{1}{K_1 + 1}} \tilde{\mathbf{h}}_{t,k}, \quad (4)$$

$$\mathbf{h}_r = \sqrt{\frac{K_2}{K_2 + 1}} \bar{\mathbf{h}}_r + \sqrt{\frac{1}{K_2 + 1}} \tilde{\mathbf{h}}_r, \quad (5)$$

Here, K_1 signifies the Rician factor for $\mathbf{h}_{t,k}$, with $\bar{\mathbf{h}}_{t,k}$ in $C^{1 \times M}$ representing the Line-of-Sight (LOS) component and $\tilde{\mathbf{h}}_{t,k}$ in $C^{1 \times M}$ as the non-Line-of-Sight (NLOS) component. Similarly, K_2 is the Rician factor for $\mathbf{h}_r$, where $\bar{\mathbf{h}}_r$ in $C^{N \times 1}$ denotes the LOS component, and $\tilde{\mathbf{h}}_r$ in $C^{N \times 1}$ represents the NLOS component. The channel between IRS$_1$ and IRS$_2$, $\mathbf{H}_{m,n} \sim \mathcal{CN}(0, \mathbf{R})$, follows the spatially correlated Rayleigh fading channel model, where $\mathbf{R}$ represents the covariance matrix that is derived according to the exponential spatial correlation model. It is controlled by the parameter ρ within the interval [0, 1], denoting the correlation coefficient among neighboring RUs, and it is given as below:

$$[\mathbf{R}]_{m,n} = \rho^{|m-n|} e^{|m-n|\theta_{i,2}}, \quad (6)$$

where $\theta_{i,2}$ is the angle of arrival between IRS$_1$ and IRS$_2$. High values of ρ, result in high correlation among $\mathbf{H}_{mn}$ elements, and in cases where ρ is less than 1 (i.e., not equal to 1), the significant correlations are between adjacent RUs only, with considerably low correlation at large distances.

Further, we assume that the channels $\mathbf{h}_{t,k}$, and $\mathbf{h}_r$ are perfectly known for all the transmitters and the R_x.

B. TRANSMITTERS AND RECEIVER ANTENNA GAINS
The gains for the users' and R_x antennas $G_t(o)$ and $G_r(o)$ are expressed as

$$G_{t,k}(o) = 4e_t \frac{J_1\left(\frac{\pi D_t \sin(o)}{\lambda}\right)}{\sin(o)}. \quad (7)$$

$$G_r(o) = 4e_r \frac{J_1\left(\frac{\pi D_r \sin(o)}{\lambda}\right)}{\sin(o)}. \quad (8)$$

Here, $J_1(\cdot)$ denotes the first-order Bessel function of the first kind, D_t stands for the antenna diameter of the T_x, and D_r stands for the antenna diameter of the R_x. The angle, measured from the broadside of the antenna, is denoted as o [14].

Thus, the maximum gain is for $o = 0$ and is denoted as

$$G_{t,k}(o) = e_t \left(\frac{\pi D_t}{\lambda}\right)^2. \quad (9)$$

$$G_r(o) = e_r \left(\frac{\pi D_r}{\lambda}\right)^2. \quad (10)$$

Here, e_t and e_r represents the aperture efficiencies for the T_x and the R_x respectively. Additionally, the gain of each RU is expressed as detailed in [14].

$$G(\theta_{i1,k}) = 4\cos(\theta_{i1,k}), \quad 0 \le \theta_{i1,k} \le \pi/2, \quad (11)$$

where $\theta_{i1,k}$ is the angle of incidence from user k to IRS$_1$ [14].

C. ANALYSIS OF LOSS FACTORS
The total losses and gains on the path between each T_{x_k} and the R_x are denoted by $L_{\tau,k}$. This includes the antenna gains, free space path loss (FSPL), and THz absorption loss (AS).

$$L_{\tau,k} = L_{FSPL,\tau,k} \, L_{abs,k}, \quad (12)$$

where $L_{abs,k}$ represents the total THz absorption losses for each T_{x_k}. The losses in the THz range are calculated based on atmospheric conditions using the simplified model suggested in [15]. $L_{FSPL,\tau,k}$ represents the total FSPL for each T_{x_k} and is denoted as

$$L_{FSPL,\tau,k} = L_{FSPL,k} \, L_{FSPL,r}. \quad (13)$$

$L_{FSPL,k}$ for the signal reflected from IRS$_1$ towards IRS$_2$ is represented as

$$L_{FSPL,k} = \frac{(\frac{\lambda}{4\pi})^2 \, G_{t,k} G_{\theta_{i1,k}} G_{\theta_r,1}}{r_{t_k}^2}, \quad (14)$$

and $L_{FSPL,r}$ between IRS$_1$ and the R_x is expressed as

$$L_{FSPL,r} = \frac{(\frac{\lambda}{4\pi})^4 \, G_{\theta_{i,2}} G_{\theta_r,2} G_r}{r_2^2 r_3^2}. \quad (15)$$

The total FSPL for each T_{x_k} is expressed as

$$L_{FSPL,\tau,k} = \left(\frac{\lambda}{4\pi}\right)^6 \frac{G_{t,k} G(\theta_{i1,k}) G(\theta_{r,1}) G(\theta_{i,2}) G(\theta_{r,2}) G_r}{r_{tk}^2 r_2^2 r_3^2}. \quad (16)$$

D. RATE OF THE DESIRED USER UNDER INTERFERENCE

The rate of the desired user under an interference scenario is expressed as

$$R_k = \log_2(1 + \gamma_k), \tag{17}$$

Here, γ_k represents the Signal-to-Interference-plus-Noise-Ratio (SINR) for user k:

$$\gamma_k = \frac{P_{Rx}^{(k)}}{\sum_{\substack{i=1 \\ i \neq k}}^{K} P_{Rx}^{(i)} + \sigma^2}, \tag{18}$$

In this equation, $P_{Rx}^{(k)}$ denotes the power received for user k, and σ^2 represents the noise variance.

1) DERIVATION OF THE USER'S RECEIVED POWER ($P_{RX}^{(K)}$)

In our setup, both users transmit at IRS_1, covering all elements of IRS_1 from different angles and distances. The power reflected from the mth RU of IRS_1 can be expressed as in [14], excluding the calculation of absorption losses.[1]

$$P_{r,m}^{(k)} = \left(\frac{\lambda}{4\pi}\right)^2 \frac{G_{t,k} G(\theta_{i1,k}) G(\theta_{r,1})}{r_{tk}^2} \times |h_{t,km}|^2 |\phi_m|^2 P_t, \tag{19}$$

Here, $\phi_m = e^{-j\eta_m}$ represents the reflection coefficient of the mth RU of IRS_1; $G_{t,k}$ denotes the antenna gain of user k at the T_x; $G(\theta_{i1,k})$ is the gain of the RU from the incident angle, $G(\theta_{r,1})$ is the gain of the RU form the reflection angle, and $r_{t,k}$ is the distance between T_{x_k} and RU m. Similarly, the power reflected from the nth RU of IRS_2 when it is illuminated by the signal reflected by the mth RU of IRS_1 can be expressed as follows:

$$P_{r,mn}^{(k)} = \left(\frac{\lambda}{4\pi}\right)^4 \frac{G_{t,k} G(\theta_{i1,k}) G(\theta_{r,1}) G(\theta_{i,2}) G(\theta_{r,2})}{r_{tk}^2 r_2^2} \times |h_{t,km}|^2 |\phi_m|^2 |H_{mn}|^2 |\phi_n|^2 P_t, \tag{20}$$

In this equation, $\phi_n = e^{-j\psi_n}$ represents the reflection coefficient of the nth RU of IRS_2, and H_{mn} denotes the (m, n) element of the channel matrix $\mathbf{H}$ connecting IRS_1 to IRS_2. The received power captured at the receiver R_x through the channel H_{mn} can be expressed as follows:

$$P_{rx,mn}^{(k)} = \left(\frac{\lambda}{4\pi}\right)^2 \frac{P_{r,mn}^{(k)}}{r_3^2} G_r |h_{rn}|^2, \tag{21}$$

and the total power received for user k at the R_x is expressed as [14]

$$P_{Rx}^{(k)} = \left| \sqrt{L_{\tau,k}} \sum_{m=1}^{M} \sum_{n=1}^{N} |h_{t,km}||H_{mn}||h_{rn}| \right. \\ \left. \times e^{-j\left(\varphi_{t_{k_m}} + \eta_m + \varphi_{mn} + \psi_n + \varphi_{r_n} + \Omega_k + \Omega_3\right)} \right|^2 P_t, \tag{22}$$

---

1. The absorption loss, $L_{abs,k}$, is included in $L_{\tau,k}$ which will show later in the expression for the total received power.

where $\varphi_{t_{k_m}}$ is the phase for the T_x channel for user k and m^{th}RU, φ_{mn} is the phase for the $\mathbf{h}_{m,n}$ channel for m^{th} and n^{th} RU, and φ_{r_n} is the phase for the R_x channel for n^{th} RU. Therefore, (22) can be re-written as

$$P_{Rx}^{(k)} = \left| \sqrt{L_{\tau,k}} \sum_{m=1}^{M} \sum_{n=1}^{N} |h_{t,km}||H_{mn}||h_{rn}| \right. \\ \left. \times e^{-j\left(\varphi_{t_{k_m}} + \eta_m + \varphi_{mn} + \psi_n + \varphi_{r_n} + \Omega_k + \Omega_3\right)} \right|^2 P_t. \tag{23}$$

Proposition 1: It can be shown that the total received power for each T_{x_k} at the R_x can be given as follows:

$$P_{Rx}^{(k)} = \left| \sqrt{L_{\tau,k}} e^{-j\Omega_3} \mathbf{h}_r^H \mathbf{\Phi}_N \mathbf{H}_{mn}^H \mathbf{\Phi}_M \mathbf{h}_{t,k}^H e^{-j\Omega_k} \right|^2 P_t. \tag{24}$$

Proof: The proof is given in the Appendix. ∎

2) DERIVATION OF THE USER'S SINR

To this end, substituting (24) in (18) leads to the below signal-to-interference-plus-noise ratio (SINR) for user 1

$$\gamma_k = \frac{\left| \sqrt{L_{\tau,k}} e^{-j\Omega_3} \mathbf{h}_r^H \mathbf{\Phi}_N \mathbf{H}_{m,n}^H \mathbf{\Phi}_M \mathbf{h}_{t,k}^H e^{-j\Omega_k} \right|^2 P_t}{\sum_{\substack{i=1 \\ i \neq k}}^{K} \left| \sqrt{L_{\tau,i}} e^{-j\Omega_3} \mathbf{h}_r^H \mathbf{\Phi}_N \mathbf{H}_{m,n}^H \mathbf{\Phi}_M \mathbf{h}_{t,i}^H e^{-j\Omega_i} \right|^2 P_t + \sigma^2}. \tag{25}$$

IV. MAXIMIZING THE RATE OF A DESIRED USER UNDER INTERFERENCE

In this section, we provide the analytical derivations of the first objective, which is maximizing the rate of a desired user, while the other user is considered an interferer. Our objective is to find the optimum phases for the multi-hop IRSs that maximize the received rate of the desired user. We will show that the rate maximization problem is non-convex and finding a closed-form expression of the IRS phases is mathematically intractable. Then we propose a sub-optimal solution to the problem through maximizing the received power of the desired user. In addition, we propose a DDPG algorithm that maximizes the rate of the desired user.

To maximize the rate of the desired user under interference, we need to solve:

$$\max_{\mathbf{\Phi}_N, \mathbf{\Phi}_M} \quad \log_2(1 + \gamma_k),$$
$$\text{s.t. } C1 : |\phi_m|^2 = 1, \forall m \in \{1, 2, \ldots, M\},$$
$$C2 : |\phi_n|^2 = 1, \forall n \in \{1, 2, \ldots, N\}, \tag{26}$$

The optimization problem presented in (27) is considered NP-hard, making the solution non-trivial due to the non-convexity arising from the constant amplitude constraints of IRS_1 and IRS_2 reflecting elements. The constant modulus constraint is a mathematical condition that restricts the square of the magnitude of a complex variable to a fixed value. This non-convexity introduces challenges in finding the global optimum, resulting in multiple local optima. Consequently, obtaining an analytical closed-form expression for the optimal phase shifts of both IRSs is mathematically

intractable. The optimal solution needs to strike a balance between enhancing the received Signal-to-Noise Ratio (SNR) for the desired user and mitigating interference from the other user, although these sub-objectives may not necessarily align. Therefore, we employ a sub-optimal approach for (27) by focusing on maximizing the power received for the desired user [13].

3) SUB-OPTIMAL SOLUTIONS: MAXIMIZING THE RECEIVED POWER OF THE DESIRED USER

To maximize the total received power of the desired user (e.g., user 1), we will solve the following system of equations:

$$\eta_m + \psi_n + \varphi_{t_{1_m}} + \varphi_{mn} + \varphi_{r_n} + \Omega_1 + \Omega_3 = \nu, \quad \forall m, n. \tag{27}$$

Here, ν is an arbitrary constant. Equation (27) can be interpreted as follows: $P_{Rx}^{(k)}$ will be maximized when the phases across all the paths established by the different IRS elements of both IRSs are constant for all m and n. Without loss of generality, we can set $\nu = 0$. Equation (27) represents an over-determined system of equations with $M + N$ unknowns (the phase shifts of the elements of IRS$_1$ and IRS$_2$) and $M \times N$ equations (corresponding to the different paths established through all combinations of the M reflective elements of IRS$_1$ and the N reflective elements of IRS$_2$).

The set of equations in (27) can be represented as:

$$\mathbf{A}\Theta = \mathbf{C}, \tag{28}$$

Here, Θ is a column vector with dimensions $(M + N) \times 1$ representing the phase shifts of IRS$_1$ and IRS$_2$, denoted as $\eta_1, \eta_2, \ldots, \eta_M, \psi_1, \psi_2, \ldots, \psi_N$. $\mathbf{A}$ is a binary matrix with dimensions $(M \times N) \times (M + N)$, and $\mathbf{C}$ is a column vector with dimensions $(M \times N) \times 1$. $\mathbf{C}$ contains known constant values, including the phase shifts of the T_x channel, $\mathbf{h}_{t,k}$, the phase shifts of the channel between IRS$_1$ and IRS$_2$, $\mathbf{H_{mn}}$, and the phase shifts of the R_x channel, $\mathbf{h}_r$. We address this problem by employing two sub-optimal mathematical techniques, namely, the P_{inv} method and the BLS. These methods allow us to determine the unknown phase shifts, η_m and ψ_n, and calculate the received power for a selected user (in this case, user 1, chosen arbitrarily as the desired user).

Pseudo-Inverse Solution: The P_{inv} solution for the over-determined system in (28) is expressed as

$$\Theta = \mathbf{A}^+ \mathbf{C}. \tag{29}$$

where $\mathbf{A}^+$ is the P_{inv} of the matrix $\mathbf{A}$ defined as

$$\mathbf{A}^+ = \left(\mathbf{A}^\mathbf{T} \mathbf{A} \right)^{-1} \mathbf{A}^\mathbf{T}, \tag{30}$$

Block Solution: Based on the spatially correlated channel assumption, a low-complexity approximate solution built on the exponential correlation model can be developed for higher values of the correlation-coefficient, ρ, between the adjacent RUs. In the case where the channel correlation is

---

Algorithm 1 Block Solution-Based Framework

1: **Input:** h_t, M, $H_{m,n}$, N, h_r, N_{blk}
2: **Output:** η_m, ψ_n, P_{Rx_k}
3: **if** $M + N \leq M \times N$ **then**
4:    Divide the elements of channel $H_{m,n}$ into blocks.
5:    **if** $M + N \geq \frac{M \times N}{N_{\text{blk}}}$ **then**
6:       Calculate the total received power using (23) by treating each group of channel elements as one block with the same value.
7:    **else**
8:       **if** $M + N < \frac{M \times N}{N_{\text{blk}}}$ **then**
9:          Solve (27) using the P_{inv} solution, and calculate the total received power using (23).
10:
11:       **endif**
12: **endif**

---

very high, the channel, $\mathbf{H_{mn}}$, can be assumed to have a block structure, where the elements in the channel matrix are organized into groups, where each group shares the same phase and exhibits no correlation between the contiguous blocks [9]. Since the number of unknowns $M + N$, the total number of IRS$_1$ and IRS$_2$ elements, is smaller than the number of equations $M \times N$, the total number of elements in the channel matrix between IRS$_1$ and IRS$_2$, then we need to reduce the number of equations. The primary concept behind the *BLS* is to minimize the number of equations by treating each group of channel elements as one block with the same value. This will result in redundant equations in the channel matrix $\mathbf{H_{m,n}}$ that can be eliminated using row reduction methods such as Gaussian elimination reducing the rank of $\mathbf{H_{m,n}}$ to the number of blocks $\frac{M \times N}{N_{\text{blk}}}$. This reduction in the rows of the channel matrix will be reflected in the equation (27) which will no longer be over-determined because the number of equations is reduced. An important point to emphasize is that the count of independent IRS$_1$ and IRS$_2$ elements remains consistent. However, through this approach, the number of equations has been streamlined from $M \times N$ to $M + N$. By employing this method, the previously over-determined system can be resolved whenever the number of blocks $\frac{M \times N}{N_{\text{blk}}} \leq M + N$.

As described in Algorithm 1, we will first check if the number of unknowns $M + N$ is less than or equal to the number of equations $M \times N$. If this condition is met, it implies that the system is over-determined. In this case, we will divide the elements of the channel matrix $\mathbf{H_{m,n}}$ into blocks. After dividing it into blocks, if the number of unknowns $M + N$ is greater or equal to the number of equations $\frac{M \times N}{N_{\text{blk}}}$, then we will calculate the total received power using the formula (23) treating each group of channel elements as one block with the same value. Else if the number of unknowns $M + N$ is still smaller than the number of equations $\frac{M \times N}{N_{\text{blk}}}$, then we will solve (27) using the P_{inv} solution, and calculate the total received power using (23).
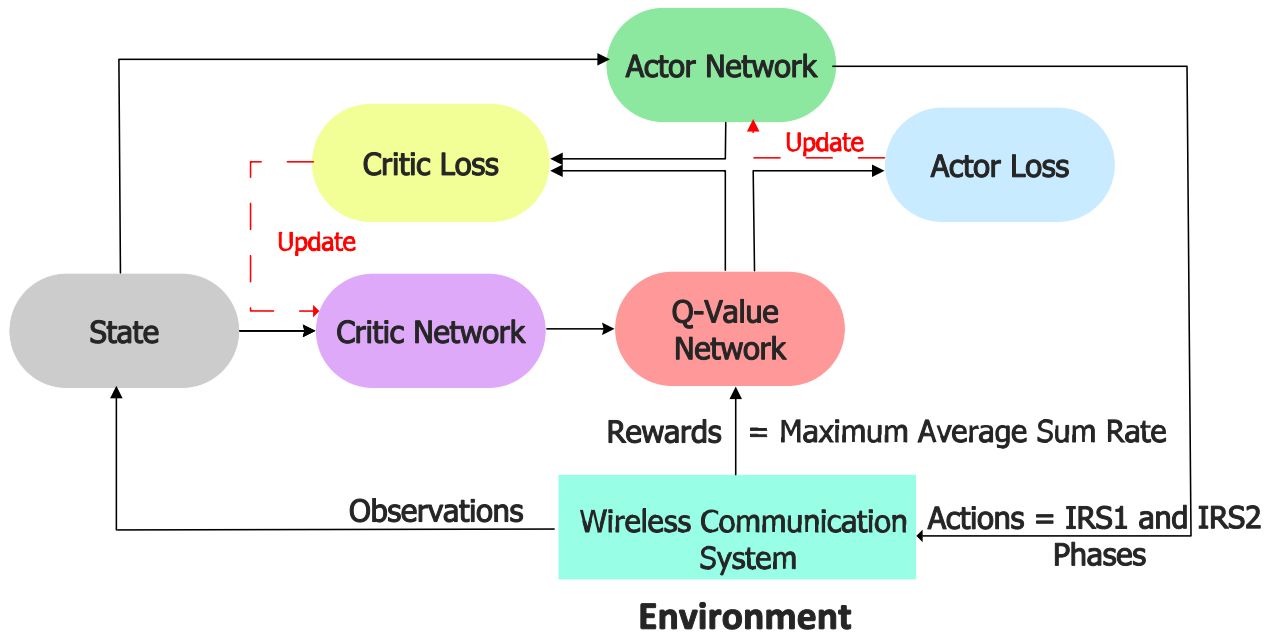
FIGURE 2. DDPG model.

Since the rate maximization problem for one of the users under interference from the other is a subset of the broader problem of maximizing the sum rate, we directly move to the latter and address the former within after establishing the DRL setup.

V. MAXIMIZING THE SUM RATE FOR BOTH USERS

In our second scenario, we aim to find the optimal phase shifts for the elements of both IRS_1 and IRS_2 to maximize the total data rate for all users at the receiver R_x, which can be formulated as follows:

$$R_{sum} = \sum_{k=1}^{K} \log_2(1 + \gamma_k). \tag{31}$$

Therefore, the problem formulated for IRS_1 and IRS_2 is to determine the phase shift matrices $\boldsymbol{\Phi}_N$ and $\boldsymbol{\Phi}_M$ that maximize the total sum rate R_{sum}, and it can be formulated as

$$\max_{\boldsymbol{\Phi}_N, \boldsymbol{\Phi}_M} \sum_{k=1}^{K} \log_2(1 + \gamma_k),$$
$$\text{s.t. } C1 : |\phi_m|^2 = 1, \forall m \in \{1, 2, \ldots, M\},$$
$$C2 : |\phi_n|^2 = 1, \forall n \in \{1, 2, \ldots, N\}, \tag{32}$$

Similar to the optimization problem presented in (27), this optimization problem is NP-hard, and finding a solution is non-trivial because of its non-convex nature caused by the constant amplitude constraints of IRS_1 and IRS_2 reflecting elements. As a result, obtaining an analytical solution is not feasible. To address this issue, we employ the Deep Reinforcement Learning (DRL) technique, specifically the DDPG algorithm, instead of attempting to solve the challenging problem through mathematical methods. Moreover, we

provide two limiting cases for the solution of this problem; an upper bound case where there is no interference and full channel phase compensation can be achieved as well as a lower bound case where phases of the elements of the IRSs are randomly chosen [13].

A. UPPER BOUND ON PERFORMANCE

Assuming the case of null interference and that the IRSs can be used to fully cancel phase shifts between different reflection paths, a relaxed upper bound on the sum rate can be established using (25), where the SINR on user k becomes

$$\gamma_k^U = \frac{\left| \sqrt{L_{\tau,k}} |\mathbf{h}_r^H| |\mathbf{H}_{m,n}^H| |\mathbf{h}_{t,k}^H| \right|^2 P_t}{\sigma^2}, \tag{33}$$

and the upper bound on the sum rate becomes

$$R_{sum}^U = \sum_{k=1}^{K} \log_2\left(1 + \gamma_k^U\right). \tag{34}$$

VI. DDPG FOR CASCADED IRS PHASE CONTROL

A. INTRODUCTION TO DDPG

In the DDPG scheme (see Fig. 2), the agents (represented by the IRSs) interacts with the environment (the communication system model) to learn an optimal policy. The state $\mathbf{s}^{(T)}$ of the agent at time step T is determined by various factors such as the received SINRs for T_{x_1} and T_{x_2} at the R_x, and the previous sum rate for both users at time step $(T-1)$. The action $\mathbf{a}^{(T)}$ taken by the agent includes the IRS_1 and IRS_2 phase shift matrices. The agent's objective is to maximize the reward $\mathbf{r}^{(T)}$, which stands for the highest sum-rate achieved. The DDPG scheme is a powerful and effective approach for solving the non-convex optimization problems in our

system. It enables the agent to learn and adapt to the dynamic environment, making it well-suited for the optimizations problems in the THz cascaded IRS system [18].

The target networks and the online networks are the two sets of networks that the DDPG algorithm uses. An actor network and a critic network are part of the online networks. At each time step, the actor network chooses an action for each state based on the input state. The actor network's choice of action is evaluated by the critic network for quality. On the other side, the target networks are utilized to increase the learning process stability. The specifications of the online networks are used to update the target networks regularly. Only a small portion of the parameters from the online networks are communicated to the target networks during the soft updates. The agent interacts with the environment by taking actions based on the current situation and receives feedback in the form of rewards during the learning process. The agent stores these experiences in a replay memory, which is a collection of past experiences. This replay memory is then used to randomly sample experiences to train the networks. The DDPG algorithm employs off-policy learning, meaning that the agent learns from past experiences stored in the replay memory rather than relying solely on the most recent experience. The weights of the networks are updated using the DDPG algorithm based on the loss function using an optimization technique, such as the Adam optimizer. The loss function is intended to maximize the expected cumulative reward (Q-value) estimated by the critic network and reduce the difference between the predicted actions and the target actions. The DDPG algorithm seeks to identify the best possible policy that maximizes the sum rate in the current environment by repeatedly updating the weights of the networks based on the accumulated experiences. The agent's learning process doesn't stop until it reaches an acceptable level of performance or convergence. The DDPG scheme is a powerful and effective approach for solving the non-convex optimization problems in (27) and (33) in our system. It enables the agent to learn and adapt to the dynamic environment, making it well-suited for the optimization of the THz cascaded IRS uplink scheme [18].

As stated earlier, the optimization problems in (27) and (33) are non-convex, and finding the optimum phases that maximize the rate through *ES* is computationally infeasible. Hence, we design DDPG solutions to find the optimum phases of the cascaded IRS. In this section, we introduce our approach using the DDPG algorithm to tackle the optimization problems outlined in equations (27) and (33) for the cascaded IRS system. Deep learning isn't a suitable fit for such a dynamic wireless communication context because it relies on the availability of training data, and deep Q-networks are also unsuitable since they are designed for discrete-time spaces exclusively. Furthermore, the convergence of the policy gradient (PG) algorithm isn't sufficient within the framework of wireless communication. The DDPG model we've chosen is well-suited for our dynamic, continuous, and non-convex wireless

communication scenario. It is designed for continuous action spaces and is well-suited for problems where the action space is not discrete. It has been applied to various continuous dynamic tasks, making it suitable for scenarios where wireless communication parameters need to be adjusted continuously [16], [17].

The primary aim of the DDPG model is to learn the policy that solves the optimization problems outlined in (27) and (33). The DDPG scheme consists of essential components: agents, states $\mathbf{s}^{(T)}$, actions $\mathbf{a}^{(T)}$, rewards $\mathbf{r}^{(T)}$, the policy function μ, and the Q-value function $Q(\mathbf{s}, \mathbf{a}|\theta^Q)$. Our agents, IRS_1 and IRS_2, operate in the environment which is the communication system, and the states $\mathbf{s}^{(T)}$ represent the received SINR for Tx_1 at R_x, the SINR for Tx_2 at R_x, and the sum rate for users at time step $(T-1)$. The actions $\mathbf{a}^{(T)}$ correspond to the phase shifts of IRS_1 and IRS_2, and the reward $\mathbf{r}^{(T)}$ is based on the received power for user 1 for our first objective and the sum rate for the users for the second objective. Our goal is to optimize the average rewards, which involve both immediate and future rewards. The DDPG scheme incorporates four *NN*s: the actor, the critic, the target actor, and the target critic networks, ensuring stability in the learning process [18].

B. DDPG SYSTEM MAPPING

The initial stage in addressing the optimization problem in our system model involves mapping it to the fundamental components of the DDPG algorithm. These components include defining the state, the action, and the reward functions. We will explore this mapping process and provide an overview of how the DDPG algorithm behaves.

1) STATE SPACE

The state space of the DDPG agent at timestep T is specified as follows:

For the first objective:

$$\mathbf{s}^{(T)} = \left[\gamma_1^{(T-1)}, \gamma_2^{(T-1)}, P_{Rx_k}^{(T-1)} \right], \qquad (35)$$

For the second objective:

$$\mathbf{s}^{(T)} = \left[\gamma_1^{(T-1)}, \gamma_2^{(T-1)}, R_{sum}^{(T-1)} \right], \qquad (36)$$

Here, $\gamma_1^{(T-1)}$, $\gamma_2^{(T-1)}$, $P_{Rx_k}^{(T-1)}$, and $R_{sum}^{(T-1)}$ represent the received SINR for T_{x_1} at the R_x, the received SINR for T_{x_2} at the R_x, and the sum rate for users at time step $(T-1)$ respectively.

2) ACTION SPACE

The actions correspond to the phase shift values assigned to IRS_1 and IRS_2 elements. These actions are expressed as an array that specifies the phase of each IRS element. Therefore, the action space is determined by the policy function as follows:

$$\mathbf{a}^{(T)} = \mu\left(\mathbf{s}^{(T)}|\theta^\mu \right) + \mathbf{n}(T) \qquad (37)$$

Here, μ represents the policy function, and θ^μ designates the weights of the *NN*, and $\mathbf{n}(T)$ describes the noise generated by the Ornstein Uhlenbeck (OU) process [19]. Given that the action space is continuous, the exploration of this space is managed using noise produced by the OU process. This involves generating noise samples from a correlated normal distribution.

3) REWARD FUNCTION

The reward function for the first objective is defined based on the maximum received power for the desired user:

$$r^{(T)} = P_{Rx_k}^{(T)} \tag{38}$$

where $P_{Rx_k}^{(T)}$ is the maximum received power for user 1. For the second objective, it is represented as the maximum sum rate for users:

$$r^{(T)} = R_{sum}^{(T)} \tag{39}$$

where $R_{sum}^{(T)}$ represents the actual sum-rate for the users.

4) DDPG SCHEME

The objective of the DDPG scheme is to train IRS$_1$ and IRS$_2$ agents to optimize their actions to maximize the average reward over the long term, which corresponds to the power received for the first user, and the sum rate of both users. These agents adapt their randomized policies and phase shift matrices to navigate the stochastic variations in the environment and ensure a consistent long-term average reward. This approach prioritizes sustained performance over immediate responses to the unpredictable fluctuations in the channel.

The DDPG implementation process is explained in Algorithm 2. Initially, we set the time step T to 0 and initialize the replay buffer $\mathcal{D}$ with a capacity of M. Then, we randomly initialize the parameters of the actor network (θ^μ) and the critic network (θ^Q). After that, we will set the target actor network parameters ($\theta^{\mu'}$) to be the same as the actor network parameters (θ^μ) and set the target critic network parameters ($\theta^{Q'}$) to be the same as the critic network parameters (θ^Q). In each iteration, IRS$_1$ and IRS$_2$ agents observe the state, which includes the received SINR for T_{x1} in the previous state, denoted as $\gamma_1^{(T-1)}$ at R_x, the received SINR for T_{x2} in the previous state, represented as $\gamma_2^{(T-1)}$ at R_x, and the reward from the previous state. Subsequently, they compute the actions $\boldsymbol{\Phi}_M$ and $\boldsymbol{\Phi}_N$ that optimize the long-term reward. The actor network is responsible for this task, while the critic network takes the state and action as inputs and produces an estimate of the expected reward, encompassing the user 1's received power and the users' sum rate. After calculating the reward, a new state is observed, and IRS$_1$ and IRS$_2$ agents adjust the phases accordingly until the system learns to achieve the optimal reward. To enhance stability, the target actor and critic networks are periodically updated based on the most recent actor and critic parameter values.

Algorithm 2 DDPG-Based Framework

1: **Initialization:** Begin by setting T to 0 and initializing the replay buffer of the DDPG agent, denoted as $\mathcal{D}$, with a capacity of M.
2: Randomly initialize the actor network weights as θ^μ and the critic network weights as θ^Q.
3: Initialize the target networks: Set $\theta^{\mu'}$ to θ^μ and $\theta^{Q'}$ to θ^Q.
4: **for** $T = 1$ to ∞ **do**
5:     Observe the current state $s^{(T)}$ and choose an action while taking into account the exploration noise generated by the OU process. $a^{(T)} = \mu(s^{(T)}|\theta^\mu) + n_T$
6:     Execute action $a^{(T)}$ at IRS$_1$ and IRS$_2$.
7:     Obtain the immediate reward $r^{(T)}$, observe the subsequent state $s^{(T+1)}$, and then record this transition as $(s^{(T)}, a^{(T)}, r^{(T)}, s^{(T+1)})$ within the reply buffer D.
8:     Select a random mini-batch of transitions from the replay buffer $\mathcal{D}$ $B \leftarrow \{(s^{(i)}, a^{(i)}, r^{(i)}, s^{(i+1)})\} \in \mathcal{D}$.
9:     Compute the targets in the following manner: $\tilde{Q}(s^{(i)}, a^{(i)}|\theta^Q) = r^{(i)} + \Gamma Q(s^{(i+1)}, \mu(s^{(i)}|\theta^{\mu'})|\theta^{Q'})$
10:     Update the parameters θ^Q in the critic network by minimizing the loss function: $L = \frac{1}{|B|} \sum_{i=1}^{|B|} \left(\tilde{Q}(s^{(i)}, a^{(i)}|\theta^{Q'}) - Q(s^{(i)}, a^{(i)}|\theta^Q) \right)^2$
11:     Adjust the parameters θ^μ in the actor network using the sampled policy gradient: $\nabla_{\theta^\mu} J \approx \frac{1}{|B|} \sum_{i=1}^{|B|} \nabla_a Q(s^{(i)}, a^{(i)}|\theta^Q) \nabla_{\theta^\mu} \mu(s^{(i)}|\theta^\mu)$
12:     Update the target actor and target critic networks: $\theta^{Q'} \leftarrow \tau\theta^Q + (1-\tau)\theta^{Q'}$ $\theta^{\mu'} \leftarrow \tau\theta^\mu + (1-\tau)\theta^{\mu'}$
13: **end for**

Further, the architecture of the DDPG algorithm consists of four *NN*s, comprising the critic and actor networks, along with the target critic and target actor networks. The role of these target networks is pivotal in improving the stability of the learning process. They are employed in the Q-target formula to estimate the value of future states, which is used to train the current networks [18].

C. COMPLEXITY ANALYSIS

To disclose the complexity of the DDPG algorithm, we demonstrate a quantitative analysis of the proposed DDPG-based scheme C_{DDPG} versus the complexity of P_{inv}, *BLS*, and *ES* methods. In our analysis, we focused on the computations performed during the exploitation stage of the DDPG algorithm to evaluate its complexity, which heavily relies on the actor network's architecture. Deep *NN*s (DNNs) consist of input, output, and concealed layers (i.e., the layers that lie between the input and output strata of a DNN). We examine several factors in our analysis, including the count of states ($\mathcal{S}$), the count of neurons within the input of each layer ($\mathcal{I}$), the count of concealed layers ($\mathcal{H}$), the count of neurons in the output of each layer ($\mathcal{O}$), and the count of actions ($\mathcal{A}$). The complexity of the input layer relates to $\mathcal{S} \times \mathcal{I}$, and the complexity of the concealed layers correlates to $\mathcal{H} \times \mathcal{I} \times \mathcal{O}$, and the complexity of the output layer is connected to $\mathcal{O} \times \mathcal{A}$. Consequently, the cumulative complexity of the DDPG scheme is expressed as follows:

$$C_{DDPG} = \mathcal{S} \times \mathcal{I} + \mathcal{H} \times \mathcal{I} \times \mathcal{O} + \mathcal{O} \times \mathcal{A}$$
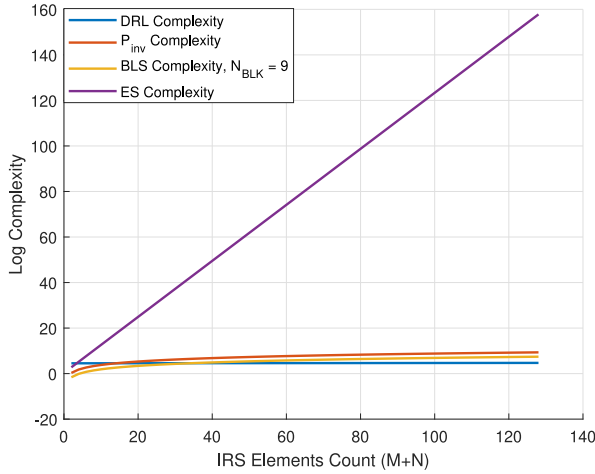
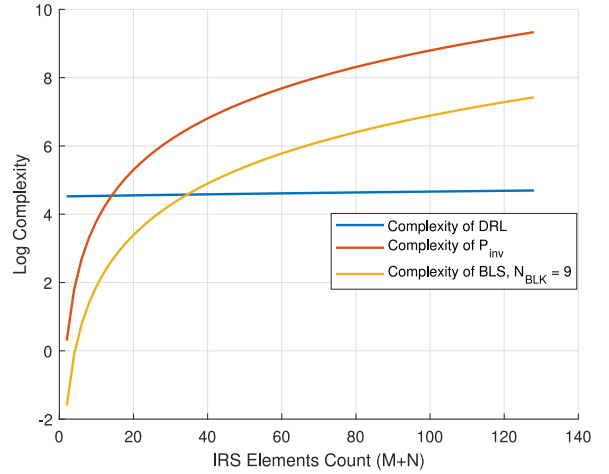**FIGURE 3.** Complexity of DRL vs. P_{inv} vs. *BLS* vs. *ES*. M = N = 64, NBLK = 9.

FIGURE 4. Complexity of DRL vs. P_{inv} vs. *BLS*. M = N = 64, NBLK = 9.

Furthermore, in the DDPG scheme, the action yielding the highest reward is always selected, and a linear search is performed on the output. Consequently, the overall computational complexity of a NN forward pass can be represented as [20]:

$$C_{DDPG} = \mathcal{S} \times \mathcal{I} + \mathcal{H} \times \mathcal{I} \times \mathcal{O} + \mathcal{O} \times \mathcal{A} + \mathcal{A}$$

Please note that the above analysis assumes a simplified perspective and doesn't consider additional factors such as activation functions, regularization techniques, or the training process itself.

In contrast, the P_{inv} solution of a matrix A with dimensions $MN \times (M + N)$ is computed using its singular value decomposition (SVD), a useful computational technique for dimensionality reduction in over-determined systems, with a complexity of $O((MN)^2 \times (M + N))$, where $MN > (M + N)$, and M and N represent IRS$_1$ and IRS$_2$ number of elements, respectively [21], [22]. On the other hand, for the BLS method, the complexity of inverting a matrix A with dimension of $\frac{MN}{N_{blk}} \times (M + N)$ is reduced to $O((\frac{MN}{N_{blk}})^2 \times (M + N))$, where $\frac{M \times N}{N_{blk}} \leq (M + N)$.

Furthermore, the complexity of the ES method (C_{ES}) is given as:

$$C_{ES} = O\left(\mathcal{K} \times \left(\left\lfloor \frac{2\pi}{\Delta \Phi} \right\rfloor + 1\right)^{(M+N)}\right), \qquad (40)$$

where $\mathcal{K}$ designates the users' count and $\lfloor \frac{2\pi}{\Delta \Phi} \rfloor$ stands for the number of phase search steps. Consequently, the DDPG algorithm shows lower complexity than that of the P_{inv}, BLS, and ES techniques as the IRS elements count increases. This relationship is illustrated in figures: Fig. 3 and Fig. 4.

VII. NUMERICAL RESULTS
In this section, we assess the performance of the suggested DDPG-based cascaded IRS-aided wireless THz communication scheme. To evaluate the DDPG system's effectiveness, we conduct a comparative analysis, focusing on two key

scenarios: one aimed at maximizing the rate for the desired user (user 1) and the other at maximizing the total rate for both users.

When optimizing the rate for the desired user, we establish two reference benchmarking schemes for our system, both utilizing 18 reflecting elements for IRS$_1$ and IRS$_2$. The first scheme relies on a P_{inv} approach, while the second employs the *BLS* method. Furthermore, for the sum rate maximization scenario, we compare the sum rates achieved using the DDPG algorithm with a discretized *ES* approximation. This comparison serves to demonstrate that the DDPG system performs closely to the *ES* method. To mitigate the computational complexity associated with the *ES*, we limit the number of reflecting elements to 4 for both IRS$_1$ and IRS$_2$. We discretize the phase shifts within the range of 0 to 2π with a search step of $2\pi/72$, resulting in $(72+1)^{(M+N)}$ possible combinations of phase shift reflection matrices. After obtaining the optimal phase shift matrices, we compute the corresponding total rate for users. Additionally, we benchmark the DDPG-derived sum rates against those calculated using random phase generation (i.e., without optimization) as an additional reference point.

A. SIMULATION PARAMETERS
The simulation parameters, as shown in Table 3, provide the details of the experimental setup, which include the use of 18 reflecting elements for both IRS$_1$ and IRS$_2$, two users ($K = 2$), each equipped with a single antenna ($N_t = 1$), and the R_x also had one antenna ($N_r = 1$). The wavelength was set at $\lambda = 10^{-3}$. The channels, encompassing the link between user 1 and IRS$_1$, user 2 and IRS$_1$, IRS$_2$, and the R_x, are characterized by a Rician fading model involving Rician factors of $K_1 = 10$ and $K_2 = 10$. The path loss exponent for the T_x to IRS$_1$ channel is 2, and the same exponent is applied to the channel between IRS$_2$ and the R_x. We selected a carrier frequency of $f = 300 \times 10^9$ and a bandwidth of $BW = 2 \times 10^9$. The noise spectral density was set to $N_{PSD} = -174 dB/Hz$, with a noise figure at the

TABLE 3. Parameters used in simulation.

Simulation Parameters	Values
Number of Users (K)	2
Number of antennas per user N_t	1
Number of antennas at the receiver N_r	1
Speed of the light c	3×10^8
Carrier Frequency f	300×10^9
Wavelength λ	1×10^{-3}
Number of IRS$_1$ (M) and IRS$_2$ (N) Reflecting Elements	18, 18
Coordinates of IRS$_1$ (x_{r1}, y_{r1}, h_{r1})	(5,10,12)
Coordinates of IRS$_2$ (x_{r2}, y_{r2}, h_{r2})	(10,10,12)
Distance between User 1 and IRS$_1$	3 to 15
Distance between User 2 and IRS$_1$	15
IRS$_1$ and IRS$_2$ Reflection Amplitudes α	1
IRS$_1$ and IRS$_2$ half-power Spacing d_x	$\lambda/2$
IRS$_1$ and IRS$_2$ Element Spacing d_y	$\lambda/2$
Antenna diameter in meters D_t	0.12
Coordinates of Rx (x_{rx}, y_{rx}, h_r)	(20,0,5)
Bandwidth	2×10^9 MHz
Noise power spectral density N_{PSD}	-174 dB/Hz
Noise figure at the receiver F_{dB}	10
Average Noise power in dB $N0$	-174 dB/Hz
Noise power in linear scale no	7.9621×10^{-11}
Transmitters to IRS$_1$ Path loss exponent	2
IRS$_2$ to receiver R_x Path loss exponent	2
Rician Factor	10
Critic Network learning rate	3×10^{-4}
Actor Network learning rate	1×10^{-4}
Target Critic Network learning rate	3×10^{-4}
Target Actor Network learning rate	1×10^{-4}
Discount factor of the future reward Γ	0.99
Coefficient of Soft Updates τ	1×10^{-3}
Batch size	128
Replay Buffer Capacity $\mathcal{C}$	10^5
Number of episodes	10000

FIGURE 5. DDPG algorithm convergence.

R_x of $F_{dB} = 10 dB$. The coordinates for IRS$_1$ were ($x_{r1} = 5$, $y_{r1} = 10$, $h_{r1} = 12$), and for IRS$_2$, the coordinates were ($x_{r2} = 10$, $y_{r2} = 10$, $h_{r2} = 12$). The distance between user 1 and IRS$_1$ varied between $r_{t1} = 3$ m and 15 m, while user 2 maintained a fixed distance of $15m$ from IRS$_1$. The coordinates of the R_x were ($x_{rx} = 20$, $y_{rx} = 0$, $h_r = 5$). The antenna diameter was set at $D_t = 0.12$ m, and the heights of user 1 and user 2 were both $h_t = 5$. We defined the distance ratio (DR) as r_{t1}, the distance from user 1 to IRS$_1$, divided by r_{t2}, the distance from user 2 to IRS$_1$. Our results were obtained through 10^3 Monte-Carlo simulations.

The suggested DDPG scheme involves two *NN*s: the actor and critic networks. Both of these networks are constructed as dense *NN*s, each comprising four layers. In these networks, each layer is a linear module with two parameters: the input size and the output size. For the actor network, the input consists of the states, with a size of 3 neurons, while the output represents the action and comprises 36 neurons. Between the input and output layers, there are two hidden layers, each with 128 neurons. These hidden layers employ the Rectified Linear Unit (ReLU) activation function. To ensure sufficient gradient information, the output layer of the actor network uses the tanh($\cdot$) activation function. As for the critic network, the input includes both the count of states and actions, which are concatenated to form the input of the critic network. Two hidden layers exist between the input layer and the output layer, with 128 neurons in each hidden layer. Again, ReLU activation functions are applied in the hidden layers. The
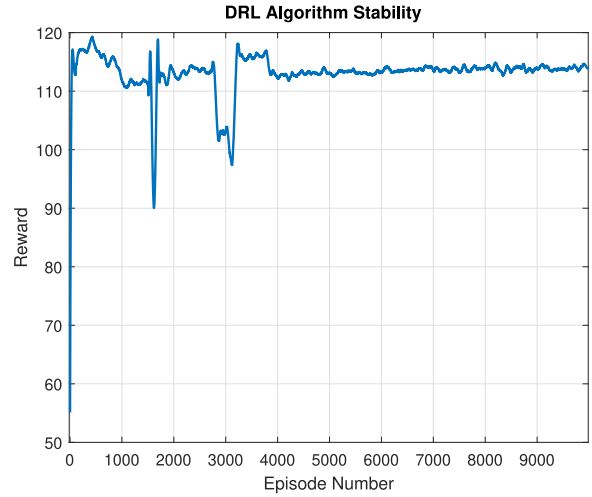
output layer of the critic network produces the Q-value and consists of 36 neurons. To update the network parameters, both the actor and critic networks use the Adam optimizer. The results are obtained by considering the average rate over 1000 iterations. The actor network is configured with a learning rate of 3×10^{-4}, while the critic network uses a learning rate of 1×10^{-4}. The discount factor for future rewards Γ is 0.99, and the batch size is set at 128. The replay buffer (denoted as $\mathcal{C}$) has a capacity of 10^5, and the number of episodes for training the model is set to 10, 000.

B. DDPG CONVERGENCE

The results depicted in Fig. 5 demonstrate the convergence of the DDPG scheme. In the figure, rewards are plotted against episodes, and it's evident that rewards increase over time, indicating a successful learning process. The DDPG algorithm learning time requires 11.53 hours for 10,000 episodes for each distance ratio value when running a single program at a time. Once trained, the implementation time for 1000 iterations is 16.421875 seconds for the DDPG, 30.6875 seconds for the Block Solution, and 947.546875 seconds for the Pinv solution. We conducted these computations on the HP EliteBook x360 830 G7 Notebook PC, featuring an Intel Core i7-10510U CPU running at 1.80GHz (2.30 GHz) and 32.0 GB of RAM.

C. MAXIMIZING THE RATE OF A DESIRED USER UNDER INTERFERENCE

1) DISTANCE RATIO IMPACT

In the scenarios aiming to maximize the rate for user 1 at the R_x, we consider different correlation factors (ρ) and DRs between user 1 and user 2. We employ various methods, including DDPG, *BLS*, and P_{inv} solution, to showcase the performance differences among them. Figures 6, 7, and 8 depict the rate of user 1 achieved with the DDPG scheme across DRs ranging from 0.2 to 1. As the DR increases, user 1's rate decreases due to the increased interference from user 2, who is getting closer to user 1.
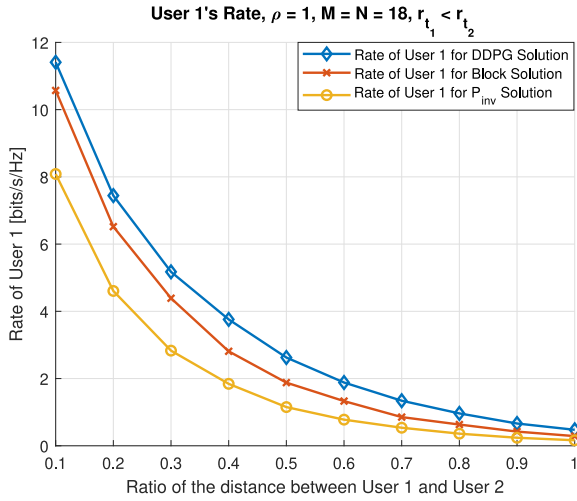
FIGURE 6. Correlation-factor ρ equal to 1.0.
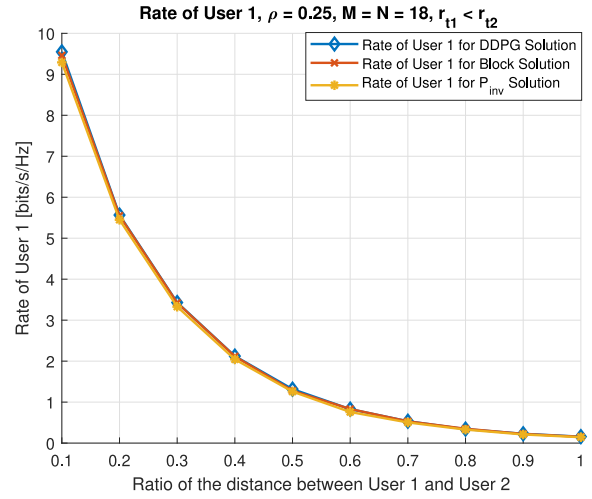
FIGURE 8. Correlation-factor ρ equal to 0.25.
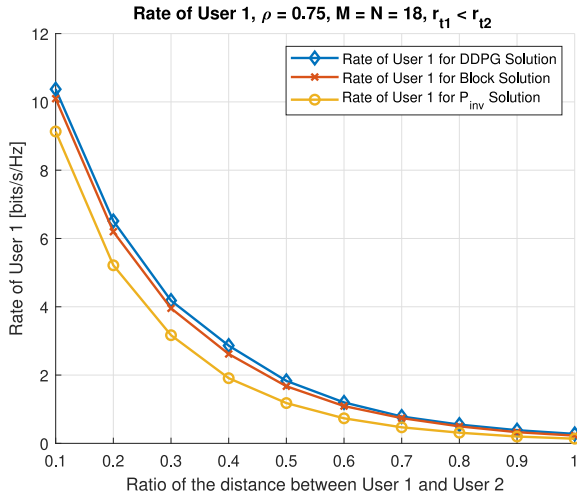
FIGURE 7. Correlation-factor ρ equal to 0.75.
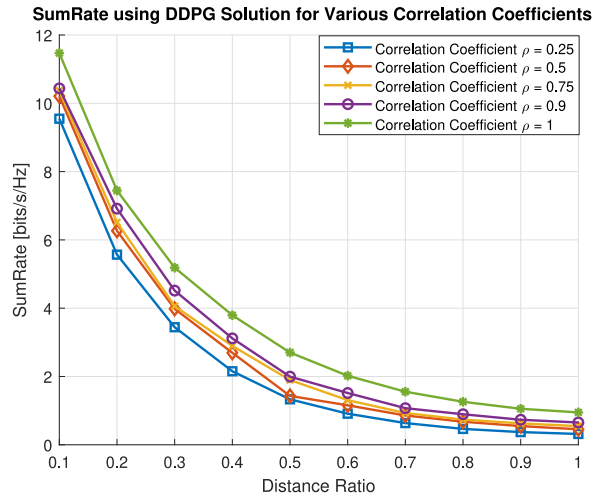
FIGURE 9. DDPG sum rate vs distance ratio for various correlation-coefficients ρ. M=N=18.

2) CORRELATION-FACTOR IMPACT

Fig. 6, Fig. 7, and Fig. 8 illustrate the behavior of user 1's data rate concerning ρ. As ρ decreases, the data rates for user 1 decrease for all methods, including DDPG, *BLS*, and P_{inv}. Conversely, when ρ increases, the data rates achieved by the DDPG technique increase as well. Thus, the enhancement in performance achieved by the DDPG algorithm over the *BLS* ranges from 8% to 57.12%, while its improvement over the P_{inv} spans from 41% to 190% for $\rho = 1$. This is due to the DDPG algorithm's improved learning efficiency with higher correlation values. Consequently, the DDPG scheme outperforms other methods, showcasing superior performance in scenarios with high correlation. This aligns with our observations, indicating that as channel correlation increases, the performance of DRL exhibits improvement, effectively leveraging the correlation for enhanced learning. These results underscore the significance of correlated channels in our scenario and their positive impact on data rates. It's important to note, however, that for low values of

ρ, the gap in data rates between DDPG and other methods retracts. Thus, for $\rho = 0.75$, the enhancement in performance achieved by the DDPG algorithm over *BLS* ranges from 2.75% to 21.6%, while its improvement over P_{inv} spans from 13.5% to 102.2%. Whereas for $\rho = 0.25$, the DDPG algorithm demonstrates a performance improvement over *BLS* ranging from 0.25% to 3%, and over P_{inv}, it spans from 2.1% to 9.7%.

D. MAXIMIZING THE SUM RATE FOR BOTH USERS
In the scenario of maximizing the sum rate for both users at the R_x, Fig. 9 displays the sum rates as a function of the DR between user 1 and user 2, using the DDPG method with various correlation coefficients ρ.

1) LEARNING RATE IMPACT
Notably, the results show that as ρ increases, the sum rates achieved with the DDPG solution also increase. It's important to highlight that constant learning rates were
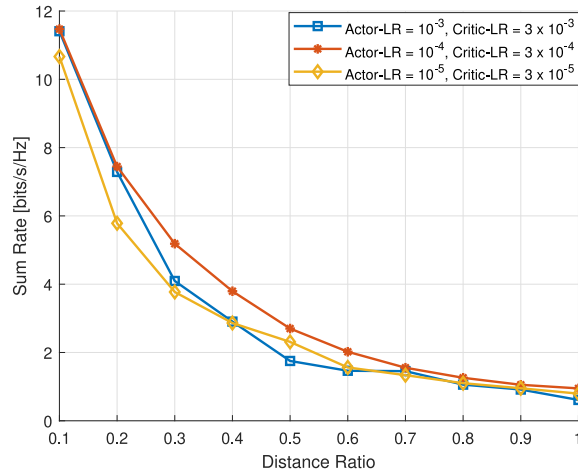
FIGURE 10. DDPG sum rate vs distance ratio for various learning rates and correlation-coefficient $\rho = 1.0$. $M = N = 18$.
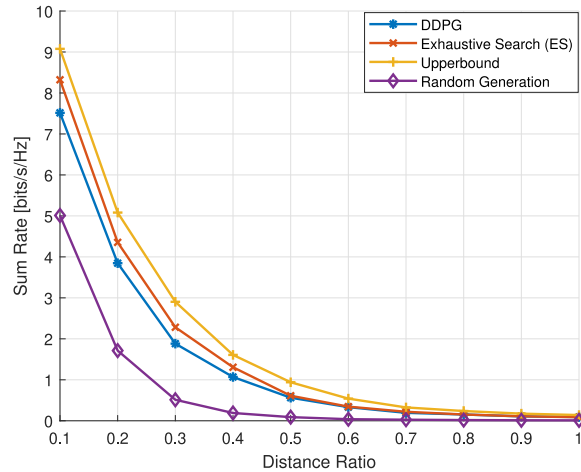

FIGURE 11. Comparison between DDPG sum rate, *ES*, and upper bound vs distance ratio for correlation-coefficient $\rho = 0.9$. $M = N = 4$.

maintained in all our simulations for the DDPG scheme, with a rate of 10^{-4} for the actor network and 3×10^{-4} for the critic network. The impact of these learning rates on the DDPG data rates is demonstrated in Fig. 10, where we compare different learning rates, including 10^{-3}, 10^{-4}, and 10^{-5} for the actor network, and 3×10^{-3}, 3×10^{-4}, and 3×10^{-5} for the critic network. The results show that the highest DDPG data rate is achieved when the learning rate for the actor networks is 10^{-4}, and for the critic networks, it's 3×10^{-4}. Therefore, these learning rates produce the best average rewards, while too small (10^{-5}) or too large (10^{-3}) learning rates result in lower average rewards. The optimal learning rate of 10^{-4} is a key factor for achieving better rewards in the DDPG scheme.

2) DDPG VS EXHAUSTIVE SEARCH

Moreover, to assess the effectiveness of our DDPG scheme, we conducted a comparison between the sum rates generated by the DDPG algorithm and those obtained through a discretized *ES* approach used to find the maximum sum rate by determining the optimal phase shift matrix. The *ES* method, while highly accurate, involves significant computational complexity. To mitigate this, we reduced the number of reflecting elements for IRS$_1$ to $M = 4$ and IRS$_2$ to $N = 4$, instead of the original $M = N = 18$. For each IRS element, we considered phase shifts ranging from 0 to 2π with a search step size of $\frac{2\pi}{72}$. Consequently, the total number of phase shift matrix combinations amounts to $(72+1)^4$. The sum rates were computed for two users across 100 Monte-Carlo simulations. The results are presented in Fig. 11, where it's evident that the DDPG algorithm's sum rates closely align with the *ES* outcomes with the specified granularity.

VIII. CONCLUSION

In this research paper, we focused on the uplink multiple access scenario within a cascaded IRS system, to address the challenges associated with short-range communications

in THz networks. Our primary goals were twofold. The first objective was to maximize the data rate for the intended user. We determined that this problem was not amenable to closed-form mathematical solutions due to its non-convex nature. As a result, we proposed two sub-optimal approaches to enhance the received power for the desired user. The second objective was to maximize the total data rate for both users, which presented a more intricate, non-convex problem. To tackle these optimization challenges, we employed DDPG algorithms, known for their effectiveness in handling non-convex optimization problems, to optimize the cascaded IRS system. The DDPG algorithm allowed us to approximate optimal IRS phase configurations that boosted the received data rate for the intended user as well as the overall data rate for both users.

Our simulation results demonstrated that, for the first objective, DDPG consistently outperformed sub-optimal methods such as P_{inv} and *BLS*, achieving higher data rates. Regarding the second objective, DDPG's achieved data rates closely matched those of a discretized *ES*, with a search step equal to $2\pi/72$. Furthermore, DDPG highlighted the importance of channel correlation in improving the learning process and achieving enhanced data rates. In summary, our paper presents a pioneering use of DDPG for optimizing cascaded IRS phase shifts, addressing an unexplored research area, and achieving superior performance.

APPENDIX

The total received signal power for each T_{x_k} at the R_x in eq. (23) can be expressed as:

$$P_{Rx}^{(k)} = |\sqrt{L_{\tau,k}} e^{-j\Omega_3} \mathbf{h}_r^H \boldsymbol{\Phi}_N \mathbf{H}_{m,n}^H \boldsymbol{\Phi}_M \mathbf{h}_{t,k}^H e^{-j\Omega_k}|^2 P_t. \quad (41)$$

Proof:

- Multiply the R_x channel $\mathbf{h}_r^H$ by IRS$_2$ phase shift reflection matrix $\boldsymbol{\Phi}_N$:

$$\left[\mathbf{h}_r^H \boldsymbol{\Phi}_N\right] = \underbrace{\left[h_{r1}^*, \ldots, h_{rm}^*, \ldots, h_{rN}^*\right]}_{1 \times N}$$

$$\times \begin{bmatrix} e^{-j\psi_1} & 0 & \cdots & \cdots & \cdots & 0 \\ 0 & e^{-j\psi_2} & 0 & \ddots & \ddots & 0 \\ \vdots & 0 & \ddots & \ddots & \ddots & \vdots \\ \vdots & & \ddots & e^{-j\psi_n} & \ddots & \vdots \\ \vdots & \ddots & & \ddots & \ddots & \vdots \\ 0 & \cdots & \cdots & \cdots & 0 & e^{-j\psi_N} \end{bmatrix}}_{N \times N} \quad (42)$$

$$\left[\mathbf{h}_r^H \boldsymbol{\Phi}_N \right] = \underbrace{\left[h_{r1}^* e^{-j\psi_1}, \ldots, h_{rn}^* e^{-j\psi_n}, \ldots, h_{rN}^* e^{-j\psi_N} \right]}_{1 \times N} \quad (43)$$

- Multiply the result of the previous operation by $\mathbf{H}_{m,n}^H$:

$$\left[\mathbf{h}_r^H \boldsymbol{\Phi}_N \mathbf{H}_{mn}^H \right] = \underbrace{\left[h_{r1}^* e^{-j\psi_1}, \ldots, h_{rn}^* e^{-j\psi_n}, \ldots, h_{rN}^* e^{-j\psi_N} \right]}_{1 \times N}$$

$$\times \underbrace{\begin{bmatrix} h_{11}^* & h_{21}^* & \cdots & \cdots & \cdots & h_{M1}^* \\ h_{12}^* & h_{22}^* & \ddots & \ddots & \ddots & h_{M2}^* \\ \vdots & \ddots & \ddots & \ddots & \ddots & \vdots \\ \vdots & \ddots & \ddots & H_{mn}^* & \ddots & \vdots \\ \vdots & \ddots & \ddots & \ddots & \ddots & \vdots \\ h_{1N}^* & \cdots & \cdots & \cdots & \cdots & h_{MN}^* \end{bmatrix}}_{N \times M} \quad (44)$$

$$\left[\mathbf{h}_r^H \boldsymbol{\Phi}_N \mathbf{H}_{mn}^H \right]$$
$$= \underbrace{\left[\sum_{n=1}^{N} h_{rn}^* e^{-j\psi_n} h_{1n}^*, \sum_{n=1}^{N} h_{rn}^* e^{-j\psi_n} h_{2n}^*, \ldots, \sum_{n=1}^{N} h_{rn}^* e^{-j\psi_n} h_{MN}^* \right]}_{1 \times M} \quad (45)$$

- Multiply the result of the previous operation by IRS$_1$ phase shift reflection matrix $\boldsymbol{\Phi}_M$:

$$\left[\mathbf{h}_r^H \boldsymbol{\Phi}_N \mathbf{H}_{mn}^H \boldsymbol{\Phi}_M \right] = \underbrace{\left[\mathbf{h}_r^H \boldsymbol{\Phi}_N \mathbf{H}_{mn}^H \right]}_{1 \times M}$$

$$\times \begin{bmatrix} e^{-j\eta_1} & 0 & \cdots & \cdots & \cdots & 0 \\ 0 & e^{-j\eta_2} & 0 & \ddots & \ddots & 0 \\ \vdots & 0 & \ddots & \ddots & \ddots & \vdots \\ \vdots & \ddots & \ddots & e^{-j\eta_m} & \ddots & \vdots \\ \vdots & \ddots & \ddots & \ddots & \ddots & \vdots \\ 0 & \cdots & \cdots & \cdots & 0 & e^{-j\eta_M} \end{bmatrix}}_{M \times M} \quad (46)$$

$$\left[\mathbf{h}_r^H \boldsymbol{\Phi}_N \mathbf{H}_{mn}^H \boldsymbol{\Phi}_M \right]$$
$$= \underbrace{\left[\sum_{n=1}^{N} h_{rn}^* e^{-j\psi_n} h_{1n}^*, \sum_{n=1}^{N} h_{rn}^* e^{-j\psi_n} h_{2n}^*, \ldots, \sum_{n=1}^{N} h_{rn}^* e^{-j\psi_n} H_{MN}^* \right]}_{1 \times M}$$

$$\times \begin{bmatrix} e^{-j\eta_1} & 0 & \cdots & \cdots & \cdots & 0 \\ 0 & e^{-j\eta_2} & 0 & \ddots & \ddots & 0 \\ \vdots & 0 & \ddots & \ddots & \ddots & \vdots \\ \vdots & \ddots & \ddots & e^{-j\eta_m} & \ddots & \vdots \\ \vdots & \ddots & \ddots & \ddots & \ddots & \vdots \\ 0 & \cdots & \cdots & \cdots & 0 & e^{-j\eta_M} \end{bmatrix}}_{M \times M} \quad (47)$$

$$\left[\mathbf{h}_r^H \boldsymbol{\Phi}_N \mathbf{H}_{mn}^H \boldsymbol{\Phi}_M \right] = \underbrace{\left[\sum_{m=1}^{M} \sum_{n=1}^{N} h_{rn}^* e^{-j\psi_n} H_{mn}^* e^{-j\eta_m} \right]}_{1 \times M} \quad (48)$$

- Multiply the result of the previous operation by the T_x channel of user K $\mathbf{h}_{t,k}^H$:

$$\left[\mathbf{h}_r^H \boldsymbol{\Phi}_N \mathbf{H}_{mn}^H \boldsymbol{\Phi}_M \mathbf{h}_{t,k}^H \right] = \underbrace{\left[\sum_{m=1}^{M} \sum_{n=1}^{N} h_{rn}^* e^{-j\psi_n} H_{mn}^* e^{-j\eta_m} \right]}_{1 \times M}$$

$$\times \underbrace{\begin{bmatrix} h_{t,k,1}^* \\ h_{t,k,2}^* \\ \vdots \\ h_{t,k,M}^* \end{bmatrix}}_{M \times 1} \quad (49)$$

$$\mathbf{h}_r^H \boldsymbol{\Phi}_N \mathbf{H}_{mn}^H \boldsymbol{\Phi}_M \mathbf{h}_{t,k}^H = \sum_{m=1}^{M} \sum_{n=1}^{N} h_{rn}^* e^{-j\psi_n} H_{mn}^* e^{-j\eta_m} h_{t,km}^* \quad (50)$$

$$\mathbf{h}_r^H \boldsymbol{\Phi}_N \mathbf{H}_{m,n}^H \boldsymbol{\Phi}_M \mathbf{h}_{t,k}^H = \sum_{m=1}^{M} \sum_{n=1}^{N} |h_{rn}| e^{-j\phi_{rn}} e^{-j\psi_n} |H_{mn}|$$
$$\times e^{-j\phi_{mn}} e^{-j\eta_m} |h_{t,km}| e^{-j\phi_{t,km}} \quad (51)$$

$$\mathbf{h}_r^H \boldsymbol{\Phi}_N \mathbf{H}_{mn}^H \boldsymbol{\Phi}_M \mathbf{h}_{t,k}^H = \sum_{m=1}^{M} \sum_{n=1}^{N} |h_{t,km}| |H_{mn}| |h_{rn}|$$
$$\times e^{-j(\phi_{t,km} + e^{-j\eta_m} + e^{-j\phi_{mn}} + e^{-j\psi_n} + \phi_{rn})} \quad (52)$$

- From the obtained result we can deduce that the total received signal power for each T_{x_k} at the R_x can be written as follows:

$$P_{Rx}^{(k)} = \left| \sqrt{L_{\tau,k}} e^{-j\Omega_3} \mathbf{h}_r^H \boldsymbol{\Phi}_N \mathbf{H}_{mn}^H \boldsymbol{\Phi}_M \mathbf{h}_{t,k}^H e^{-j\Omega_k} \right|^2 P_t,$$

$$= \left| \sqrt{L_{\tau,k}} \sum_{m=1}^{M} \sum_{n=1}^{N} |h_{t,km}| |H_{mn}| |h_{rn}| \right.$$
$$\left. \times e^{-j\left(\varphi_{t_{k_m}} + \eta_m + \varphi_{mn} + \psi_n + \varphi_{r_n} + \Omega_k + \Omega_3 \right)} \right|^2 P_t \quad (53)$$

■

REFERENCES

[1] C. Chaccour, M. N. Soorki, W. Saad, M. Bennis, P. Popovski, and M. Debbah, "Seven defining features of terahertz (THz) wireless systems: A fellowship of communication and sensing," *IEEE Commun. Surveys Tuts.*, vol. 24, no. 2, pp. 967–993, 2nd Quart., 2022, doi: 10.1109/COMST.2022.3143454.

[2] R. Imran, M. Odeh, N. Zorba, and C. Verikoukis, "Quality of experience for spatial cognitive systems within multiple antenna scenarios," *IEEE Trans. Wireless Commun.*, vol. 12, no. 8, pp. 4153–4161, Aug. 2013, doi: 10.1109/TWC.2013.071113.122037.

[3] I. Yildirim, A. Uyrus, and E. Basar, "Modeling and analysis of reconfigurable intelligent surfaces for indoor and outdoor applications in future wireless networks," *IEEE Trans. Commun.*, vol. 69, no. 2, pp. 1290–1301, Feb. 2021, doi: 10.1109/TCOMM.2020.3035391.

[4] Z. Chen, X. Ma, C. Han, and Q. Wen, "Towards intelligent reflecting surface empowered 6G terahertz communications: A survey," *China Commun.*, vol. 18, no. 5, pp. 93–119, May 2021, doi: 10.23919/JCC.2021.05.007.

[5] T. V. Nguyen, T. P. Truong, T. M. T. Nguyen, W. Noh, and S. Cho, "Achievable rate analysis of two-hop interference channel with coordinated IRS relay," *IEEE Trans. Wireless Commun.*, vol. 21, no. 9, pp. 7055–7071, Sep. 2022, doi: 10.1109/TWC.2022.3154372.

[6] W. Mei and R. Zhang, "Multi-beam multi-hop routing for intelligent reflecting surfaces aided massive MIMO," *IEEE Trans. Wireless Commun.*, vol. 21, no. 3, pp. 1897–1912, Mar. 2022, doi: 10.1109/TWC.2021.3108020.

[7] Q. Sun, P. Qian, W. Duan, J. Zhang, J. Wang, and K.-K. Wong, "Ergodic rate analysis and IRS configuration for multi-IRS dual-hop DF relaying systems," *IEEE Commun. Lett.*, vol. 25, no. 10, pp. 3224–3228, Oct. 2021, doi: 10.1109/LCOMM.2021.3100347.

[8] Z. Zhang and Z. Zhao, "Weighted sum-rate maximization for multi-hop RIS-aided multi-user communications: A minorization-maximization approach," in *Proc. IEEE 22nd Int. Workshop Signal Process. Adv. Wireless Commun. (SPAWC)*, 2021, pp. 106–110, doi: 10.1109/SPAWC51858.2021.9593114.

[9] A. Almohamad, M. Hasna, N. Zorba, and T. Khattab, "Performance of THz communications over cascaded RISs: A practical solution to the over-determined formulation," *IEEE Commun. Lett.*, vol. 26, no. 2, pp. 291–295, Feb. 2022, doi: 10.1109/LCOMM.2021.3132655.

[10] C. Huang et al., "Hybrid beamforming for RIS-empowered multi-hop terahertz communications: A DRL-based method," in *Proc. IEEE Globecom Workshops (GC)*, Taipei, Taiwan, 2020, pp. 1–6, doi: 10.1109/GCWkshps50303.2020.9367503.

[11] C. Huang et al., "Multi-hop RIS-empowered terahertz communications: A DRL-based hybrid beamforming design," *IEEE J. Sel. Areas Commun.*, vol. 39, no. 6, pp. 1663–1677, Jun. 2021, doi: 10.1109/JSAC.2021.3071836.

[12] C. Soni and N. Gupta, "Channel estimation of spatial correlated channel in massive MIMO," in *Proc. 8th Int. Conf. Comput. Sustain. Global Develop.*, New Delhi, India, 2021, pp. 836–841.

[13] K. Feng, Q. Wang, X. Li, and C.-K. Wen, "Deep reinforcement learning based intelligent reflecting surface optimization for MISO communication systems," *IEEE Wireless Commun. Lett.*, vol. 9, no. 5, pp. 745–749, May 2020, doi: 10.1109/LWC.2020.2969167.

[14] K. Ntontin et al., "Reconfigurable intelligent surface optimal placement in millimeter-wave communications," in *Proc. 15th Eur. Conf. Antennas Propag. (EuCAP)*, Dusseldorf, Germany, 2021, pp. 1–5, doi: 10.23919/EuCAP51087.2021.9411076.

[15] J. Kokkoniemi, J. Lehtomäki, and M. Juntti, "Simplified molecular absorption loss model for 275–400 gigahertz frequency band," in *Proc. 12th Eur. Conf. Antennas Propag. (EuCAP)*, 2018, pp. 1–5, doi: 10.1049/cp.2018.0446.

[16] M. Shehab, B. S. Ciftler, T. Khattab, M. M. Abdallah, and D. Trinchero, "Deep reinforcement learning powered IRS-assisted downlink NOMA," *IEEE Open J. Commun. Soc.*, vol. 3, pp. 729–739, 2022, doi: 10.1109/OJCOMS.2022.3165590.

[17] C. Huang, R. Mo, and C. Yuen, "Reconfigurable intelligent surface assisted multiuser MISO systems exploiting deep reinforcement learning," *IEEE J. Sel. Areas Commun.*, vol. 38, no. 8, pp. 1839–1850, Aug. 2020, doi: 10.1109/JSAC.2020.3000835.

[18] V. François-Lavet, P. Henderson, R. Islam, M. Bellemare, and J. Pineau, "An introduction to deep reinforcement learning," *Found. Trends Mach. Learn.*, vol. 11, nos. 3–4, pp. 1–140, 2018.

[19] G E. Uhlenbeck and L S. Ornstein, "On the theory of the Brownian motion," *Revista Latinoamericana De Microbiologia*, vol. 36, no. 5, p. 823, 1930.

[20] M. Elsayed, A. Badawy, A. E. Shafie, A. Mohamed, and T. Khattab, "A deep reinforcement learning framework for data compression in uplink NOMA-SWIPT systems," *IEEE Internet Things J.*, vol. 9, no. 14, pp. 11656–11674, Jul. 2022, doi: 10.1109/JIOT.2021.3131524.

[21] W. Keller-Gehrig, "Fast algorithms for the characteristic polynomial," *Theoretical Comput. Sci.*, vol. 36, nos. 2–3, pp. 309–317, 1985. [Online]. Available: http://dx.doi.org/10.1016/0304-3975(85)90049-0

[22] V. Vasudevan and M. Ramakrishna, "A hierarchical singular value decomposition algorithm for low rank matrices," 2017, *arXiv:1710.02812v2*.